IOPscience iopscience.iop.org

Home Search Collections Journals About Contact us My IOPscience

Impact of Source/Drain Junction and Cell Shape on Random Telegraph Noise in NAND Flash Memory

This content has been downloaded from IOPscience. Please scroll down to see the full text.

2013 Jpn. J. Appl. Phys. 52 074201

(http://iopscience.iop.org/1347-4065/52/7R/074201)

View the table of contents for this issue, or go to the journal homepage for more

Download details:

IP Address: 140.113.38.11
This content was downloaded on 25/04/2014 at 09:27

Please note that terms and conditions apply.

Japanese Journal of Applied Physics **52** (2013) 074201 **REGULAR PAPER**
http://dx.doi.org/**10.7567/JJAP.52.074201**

Impact of Source/Drain Junction and Cell Shape on Random Telegraph Noise in NAND Flash Memory

Fu-Hai Li[1*] and Riichiro Shirota[1,2]

[1] *Institute of Communications Engineering, National Chiao Tung University, Hsinchu 300, Taiwan*
[2] *Department of Electrical and Computer Engineering, National Chiao Tung University, Hsinchu 300, Taiwan*
E-mail: linaungtgi@gmail.com

Received April 26, 2013; accepted May 20, 2013; published online July 1, 2013

A comprehensive numerical study of threshold voltage fluctuation (ΔV_T) in scaled NAND flash memory caused by random telegraph noise (RTN) and discrete dopant fluctuation (RDF) in both the channel and the cell-to-cell space [source/drain (S/D)] region was carried out. Following a three-dimensional (3D) Monte Carlo (MC) procedure, the statistical distribution of ΔV_T is estimated, considering the effects of both the random placement of discrete doping atoms and a discrete single trap at the tunnel oxide/substrate interface. The result demonstrates the significant influence of the doping in the S/D regions. For the cells with and without an S/D junction, the electron concentration in the S/D region is determined by the pass voltage of the unselected cell (V_{pass}) and the neighboring cell V_T ($V_{T(n)}$), owing to the fringing fields of neighboring floating gates (FGs). As a result, ΔV_T increases in the S/D region as $V_{pass} - V_{T(n)}$ decreases. The fluctuation amplitude strongly depends on the [single-trap RTN] position along the cell length (L) and width (W) directions. For the cell shape with rounding of the active area (AA) at the shallow trench isolation (STI) edge, the results indicate that the high ΔV_T area moves from the AA edge towards the center area along the W-direction.
© 2013 The Japan Society of Applied Physics

1. Introduction

Recent NAND Flash scaling trends have already been extended below 25 nm. The threshold voltage fluctuation (ΔV_T) caused by random telegraph noise (RTN) produces severe reliability problems in the read operation of NAND Flash memory as the cell size is scaled down. Consequently, it is widely considered that RTN affects cell reliability.[1–11) Owing to the capture and emission of an electron at the trap state in the tunnel-oxide layer, RTN causes changes in both conducting carrier number and mobility. Previous research has attributed V_T distribution widening by RTN to the percolation effect due to atomistic doping spread and trap location above the channel current paths.[12–16) Statistics of the V_T instability can be examined by analyzing the cumulative distribution of ΔV_T.[17)

Both channel and source/drain (S/D) regions must be considered when examining how RTN affects NAND Flash memory. It is well known that omit to avoid program disturbance, the scaled cell gate length cannot increase the boron channel doping concentration. Correspondingly, the S/D doping must be reduced to suppress short channel effect (SCE) and program disturbance,[18–22) thus warranting a more thorough investigation of RTN for the cell with low or eliminated S/D doping levels. Even without S/D doping, fringing fields induced by neighboring floating gates (FGs) can produce an adequate number of surface electrons and achieve a sufficient string ON-current level.[23–26)

Several RTN-related studies involving SCE, S/D implantation,[18,21) channel doping, cell shape,[27–29) and adjacent cell interference have been performed recently.[30,31) Analyzing how RTN affects S/D regions is a priority concern owing to the reduction of S/D doping when the cell size is scaled down to sub-25 nm. However, to the best of our knowledge, exactly how the cell-to-cell S/D region affects RTN with various cell geometries and V_{pass} in the NAND Flash string has not yet been explored.

By three-dimensional (3D) technology computer aided design (TCAD) simulations, in this work we simulated a complete discrete-acceptor and discrete-donor dopant profile with the RTN trap for the NAND Flash string. The RTN distribution amplitudes are also investigated with and without the S/D junction, where various V_{pass} values and different cell shapes are considered. The results of this study remain valid, despite the fact that the feature size of cell dimensions approaches 15 nm. Therefore, the results of this study will contribute to the improvement of the V_T distribution widening by RTN for the further scaled down NAND Flash memory.

2. Simulation Method

The statistical distribution of V_T fluctuation amplitude is studied by performing a large number of 3D numerical simulations with a random placement of discrete acceptor (RDA) and donor (RDD) atoms, and a single electron trap at the tunnel oxide/substrate interface (Fig. 1). Cell width and length are set to 22 nm, and the substrate average boron doping concentration of 1×10^{18} cm^{-3} is implemented. Two S/D profiles are prepared: one without S/D doping (S/D junctionless) and the other with a Gaussian profile of an arsenic implant with a low peak concentration of 1×10^{18} cm^{-3}. The coupling ratio (FG to control gate capacitance divided by the total capacitance) is set to 0.6 with 8-nm-thick SiO_2 as the FG oxide. The statistical distribution of the V_T fluctuation amplitude of a read cell is then obtained using the Monte Carlo (MC) procedure.[27,28) Conventionally, with a highly doped S/D, the RTN effect arising only in the channel region has been studied.[27–30) However, considering the recent S/D doping level reduction trend, both the channel region and S/D region should be taken into account. Figure 1 shows the RTN trap placement site (RTN region), deliberately extended over the channel and cell-to-cell S/D area. The V_T value of a selected cell is extracted as the world line (WL) bias (voltage) that elicits a bit line (BL) current I_{BL} of 100 nA. The BL and source line (SL) bias as are set to 0.1 and 0 V, respectively. All cells in the NAND string are assumed to be in the neutral state (i.e., no charge placed in FG). Additionally, RTN instabilities are examined, in which the statistical distribution of the single-trap fluctuation amplitude was considered, which was shown in Ref. 13

 © 2013 The Japan Society of Applied Physics

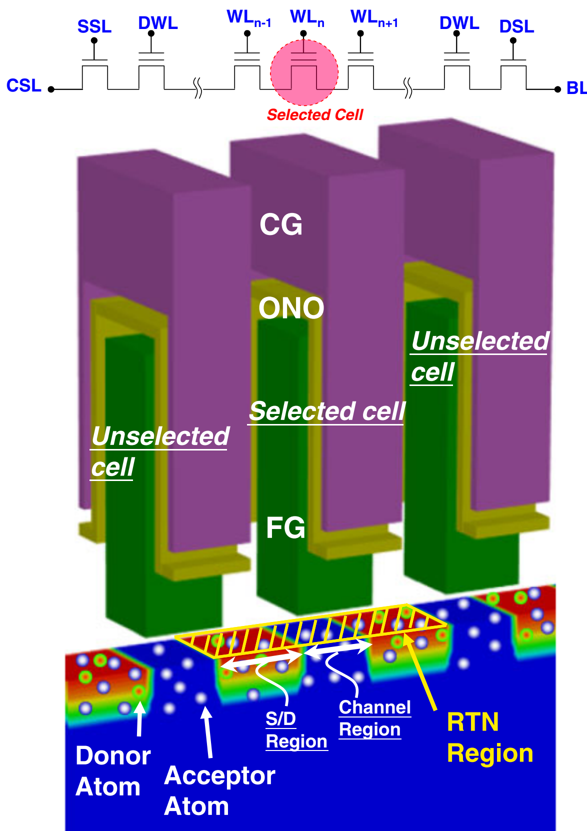

Fig. 1. (Color online) Schematic view of NAND Flash memory string with S/D junction. The RTN region and random discrete acceptor and donor atoms are highlighted. The RTN region deliberately extended over the channel region and the S/D region is shown.

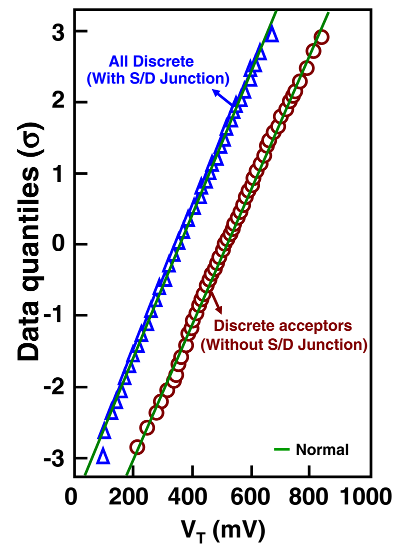

Fig. 2. (Color online) MC results for average V_T distribution of RDF. RDAs are estimated for the cell without S/D junction and all discrete cases are estimated for the cell with an S/D junction. RDAs and RDDs are added to all discrete cases. Gaussian behaviors of neutral V_T distribution are shown.

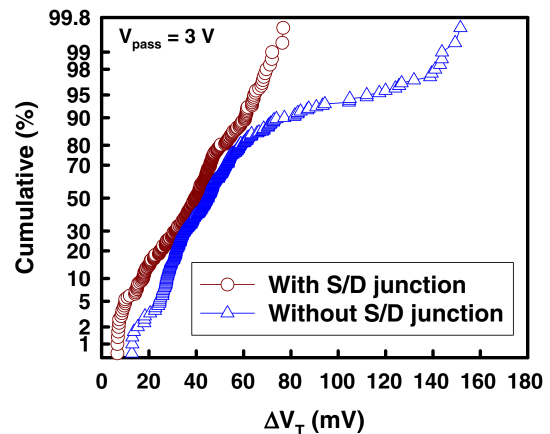

Fig. 3. (Color online) Cumulative distribution of ΔV_T for cells with and without S/D junction.

to be sufficient for an adequate description of NAND Flash memory. A single negative charge, which represents a trapped electron, is randomly placed in the channel or cell-to-cell S/D region (refer to Fig. 1 RTN region) at the tunnel-oxide/substrate interface, where its electrostatic property impacts the magnitude of the corresponding bit-line current reduction. 3D drift-diffusion simulation is carried out to estimate the I_{BL}–V_{SCG} (V_{SCG}: selected cell CG bias) trans-characteristic with the trap empty (neutral) or filled (negatively charged) by one electron. Consequently, ΔV_T is extracted as the V_T difference between the case of a negatively charged state and a neutral trap state, which is randomly placed in the channel or cell-to-cell S/D region. More than 1000 MC runs are performed for each computation. The string current that is forced through a few narrow channels connecting SL to BL is greatly influenced by the positioning of discrete dopant atoms. The Coulomb potential associated with each impurity atom acts as a barrier for the current flow. Such current channels can be completely blocked by an electron trapped near one of them, causing a large I_{BL} or V_T variation.

3. Results and Discussion

Figure 2 shows the simulated Gaussian behavior of neutral V_T distribution due to the random dopant fluctuation (RDF), where simulation is performed with and without an S/D junction. Discrete acceptors are randomly distributed in both cases, and discrete donors are added to the case of the S/D junction. Figure 3 shows a comparison between cells with and without an S/D junction in terms of the cumulative distribution of ΔV_T. Under the condition of $V_{pass} = 3$ V, ΔV_T of the S/D junctionless cell is larger than that of a cell with S/D doping. In the S/D junctionless cell, the fringing fields of the neighboring FG heavily influence the electron density in the S/D region. Consequently, a single electron trap more significantly impacts the S/D junctionless cell under a low V_{pass}. Figures 4(a) and 4(b) demonstrate the statistical contour plots of the ΔV_T distribution, as a function of the electron trap position along the L- and W-directions. Figure 4 provides insight into the origin of the tail bits shown in Fig. 3. For the S/D junctionless cell shown in Fig. 4(b), ΔV_T is significantly larger in the S/D region than in the channel region, owing to the reduced electron density in the cell-to-cell S/D area. The data pattern of the neighboring cell must be considered as well. Figure 5 shows a

 © 2013 The Japan Society of Applied Physics

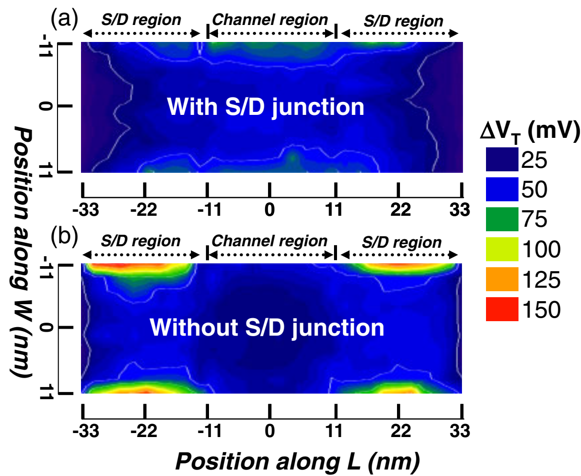

Fig. 4. (Color online) Statistical contour plots of ΔV_{T} distribution as a function of single-trap position along the L- and W-directions for cells (a) with and (b) without S/D junction.

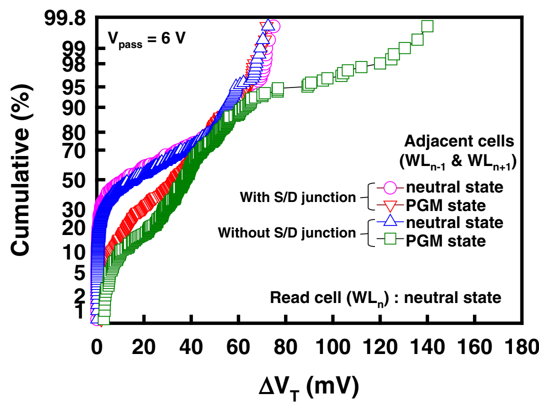

Fig. 5. (Color online) Simulated ΔV_{T} statistical distribution for cells with and without S/D junction. Adjacent cells are in a neutral or PGM state. V_{T} of programmed adjacent cells is 3 V.

comparison of the RTN results when adjacent cells are in neutral ($V_{T(n)} = 0.3$ V) and program (PGM) ($V_{T(n)} = 3$ V) states. Comparison between Figs. 3 and 5 reveals that the ΔV_{T} distribution under high $V_{T(n)}$ and V_{pass} ($V_{T(n)} = 3$ V, $V_{pass} = 6$ V) is nearly the same as that under low $V_{T(n)}$ and V_{pass} ($V_{T(n)} = 0.3$ V, $V_{pass} = 3$ V). This observation is attributed to the electron density in the S/D region being almost determined by $V_{pass} - V_{T(n)}$. Therefore, exactly how $V_{T(n)}$ and V_{pass} affect can be written simply as $V_{pass} - V_{T(n)}$, allowing us to resolve the adjacent cell interference effect by varying V_{pass} with all neighboring cells in neutral states. Figures 6(a) and 6(b) show the cumulative distribution of ΔV_{T} as a function of V_{pass} for cells with and without an S/D junction. These figures reveal that the cumulative distribution of ΔV_{T} under low V_{pass} ($V_{pass} = 3$ V) is the broadest. In particular, in the case of an S/D junctionless cell, the RTN effect significantly worsens at the tail. Thus, the V_{T} fluctuation amplitude is larger in the S/D region as $V_{pass} - V_{T(n)}$ becomes smaller. To estimate the contribution of the channel region and S/D region to ΔV_{T}, the origin of the detected severe RTN effect under various V_{pass} conditions is determined by separately simulating a single-trap in the

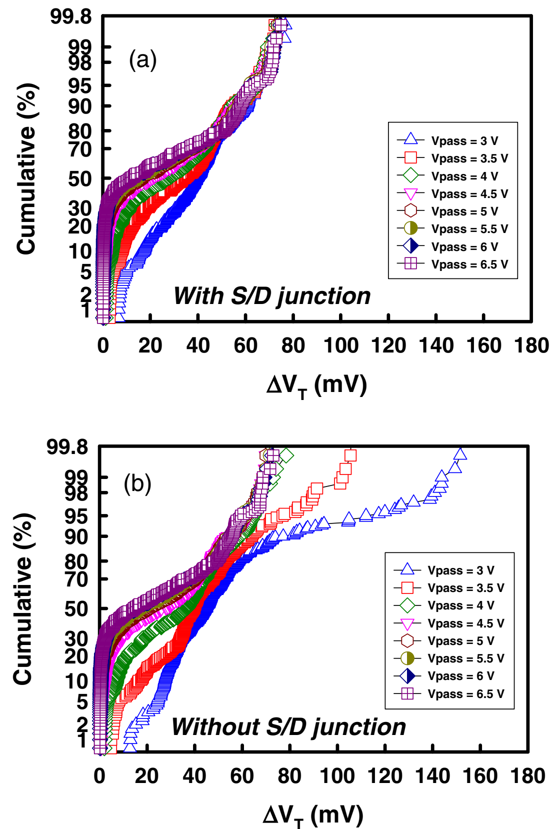

Fig. 6. (Color online) Cumulative distribution of ΔV_{T} as a function of V_{pass} for cells (a) with and (b) without S/D junction.

channel region and S/D region (Fig. 7). Figures 7(a) and 7(b) show a cell with an S/D junction, while Figs. 7(c) and 7(d) show the S/D junctionless cell in the channel region and S/D region, respectively, under various V_{pass} conditions. ΔV_{T} slightly increases with increasing V_{pass} in the channel region [Figs. 7(a) and 7(c)]. Nevertheless, Figs. 7(b) and 7(d) demonstrate that ΔV_{T} significantly decreases with increasing V_{pass} in the S/D region. This reduction is attributed to the fact that a higher electron can be induced by the fringing field of the neighboring FG, resulting in less impact on ΔV_{T} in the S/D region. Figures 8(a) and 8(b) demonstrate the statistical contour plots of the ΔV_{T} distribution along the L- and W-directions with and without the S/D junction, at various V_{pass} values. These figures reveal that V_{pass} heavily influences the extent to which the S/D region affects RTN. Figure 9 shows the average values of ΔV_{T} from the cumulative distribution of ΔV_{T} in Figs. 6 and 7. The average ΔV_{T} is extracted from the contribution of 1) the channel region, 2) the S/D region, and 3) both the channel and S/D regions. The simulation is executed by distributing a single trap randomly in each region. The RTN effect along the W-direction must also be considered. A high ΔV_{T} is crowded at the active-area edges (AA) along the W-direction (Fig. 8). In other words, the RTN effect without an S/D junction strongly depends on $V_{T(n)}$ under constant V_{pass}.

Next, the dependence of cell geometry on the ΔV_{T} distribution is considered. The RTN effect with different cell shapes (i.e., rounding of the FG and AA) is estimated by simulating three cell shapes. Figures 10(a)–10(c) show the cross-sectional views along the L- and W-directions with

 © 2013 The Japan Society of Applied Physics

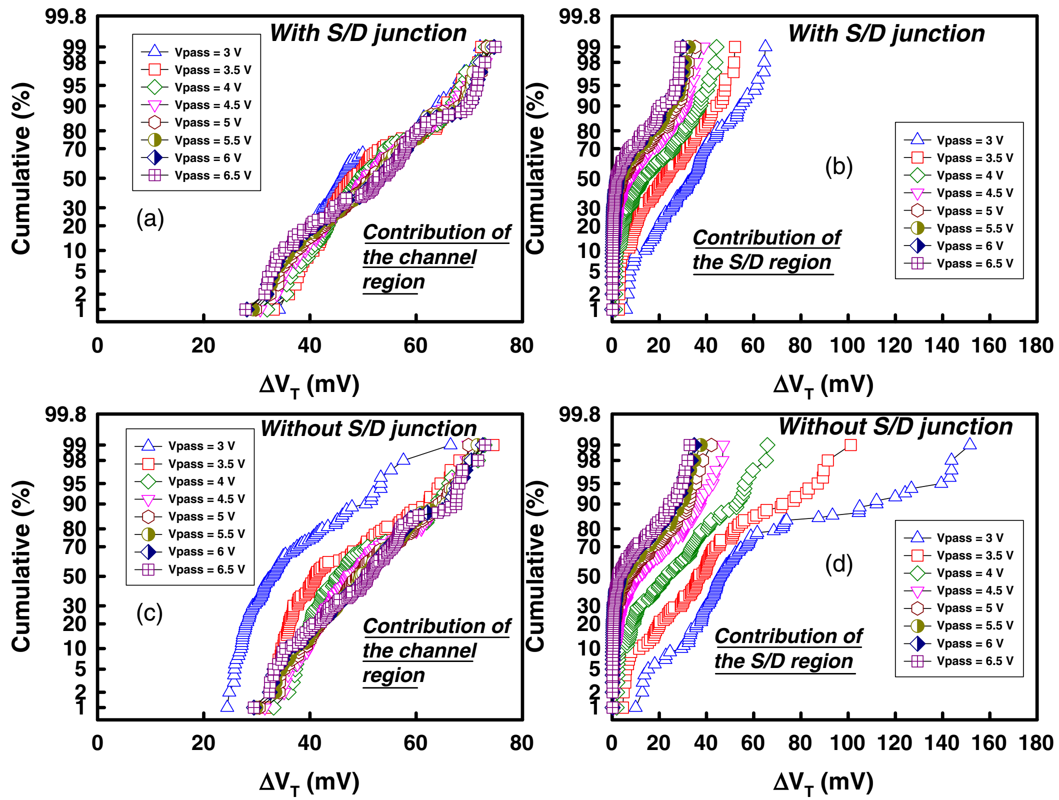

Fig. 7. (Color online) Contribution of the channel region and S/D region to ΔV_T is simulated under various V_{pass} conditions. (a) and (b) are for the cell with S/D junction. (c) and (d) are for the cell without S/D junction.

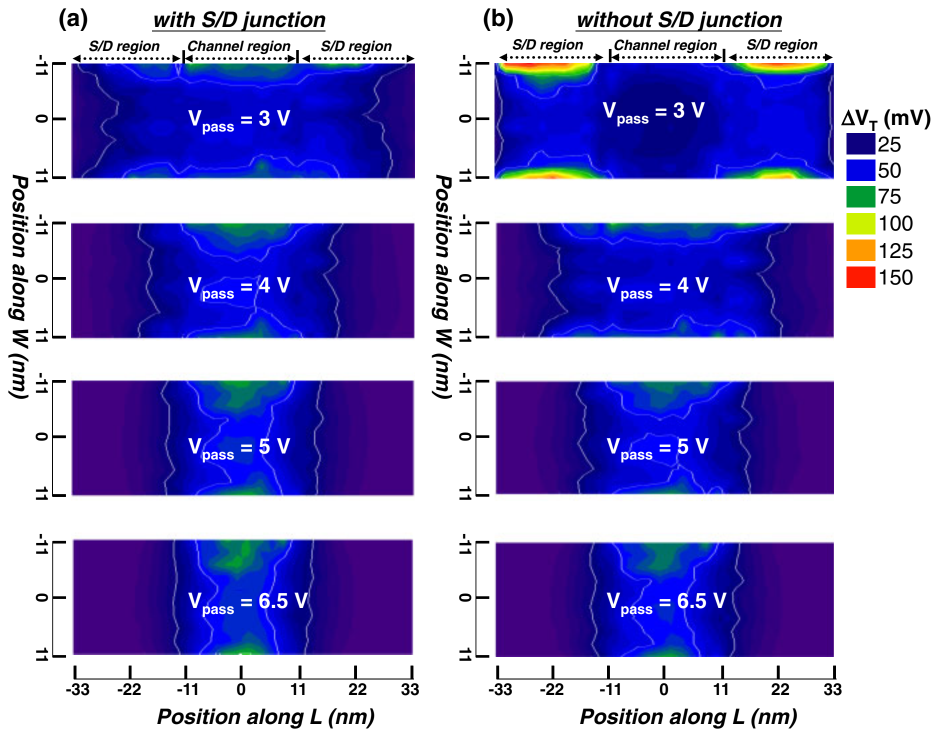

Fig. 8. (Color online) Statistical contour plots of ΔV_T distribution as a function of single-trap position along the L- and W-directions for cells (a) with and (b) without S/D junction under various V_{pass} conditions.

three cell shapes. The fluctuation amplitude ΔV_T of a single-trap RTN source is obtained by estimating cell V_T with and without a single electron randomly placed over the channel or cell-to-cell S/D region at its interface with the tunnel oxide (refer to Fig. 1, RTN region) for each cell shape. ΔV_T caused by RTN is observed following the MC procedure, considering ensembles of more than 1000 atomistically different devices for each cell shape. Case A represents a

© 2013 The Japan Society of Applied Physics

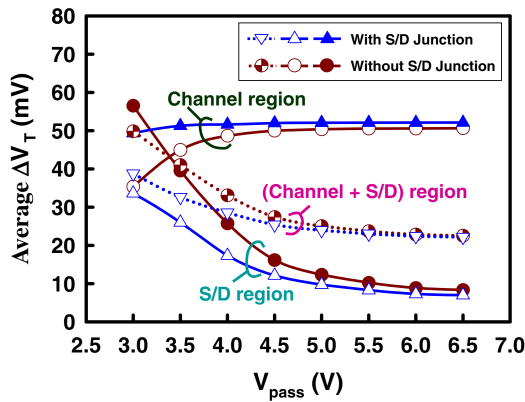

Fig. 9. (Color online) Summary of the average ΔV_T as a function of V_{pass} in the channel region, the S/D region, and the summation of the channel and S/D regions for cells with and without S/D junction.

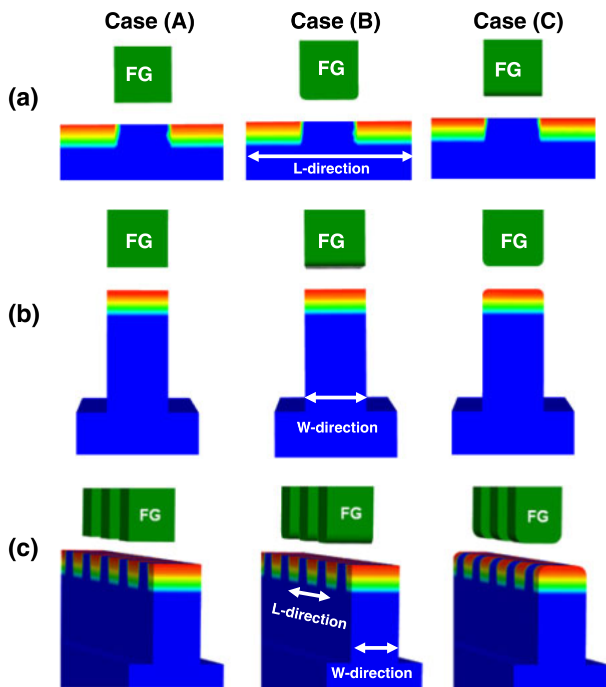

Fig. 10. (Color online) Cross-sectional views along (a) L-direction, (b) W-direction, and (c) L- and W-directions: case A (fully planar), case B (both floating-gate edges rounded along L-direction), and case C (rounded floating-gate and active-area edges along W-direction).

sharp-edge device with the fully planar AA. In the case of B, corner rounding occurs at FG edges along the L-direction. In the case of C, corner rounding occurs at both FG and AA edges along the W-direction. Case A has a uniform tunnel-oxide thickness over the entire AA, resulting in a strong electric field and current crowding at the AA edges. Case C exhibits a strong electric field and current crowding in the middle of the channel due to the AA edges rounding along the W-direction. Figures 11(a) and 11(b) show the cumulative distribution of ΔV_T with and without an S/D junction at the channel region and S/D region under a low V_{pass} ($V_{pass} = 3$ V). Simulation results indicate that the cell geometry does not significantly impact RTN. Notably, ΔV_T in the S/D region plays a dominant role in the S/D

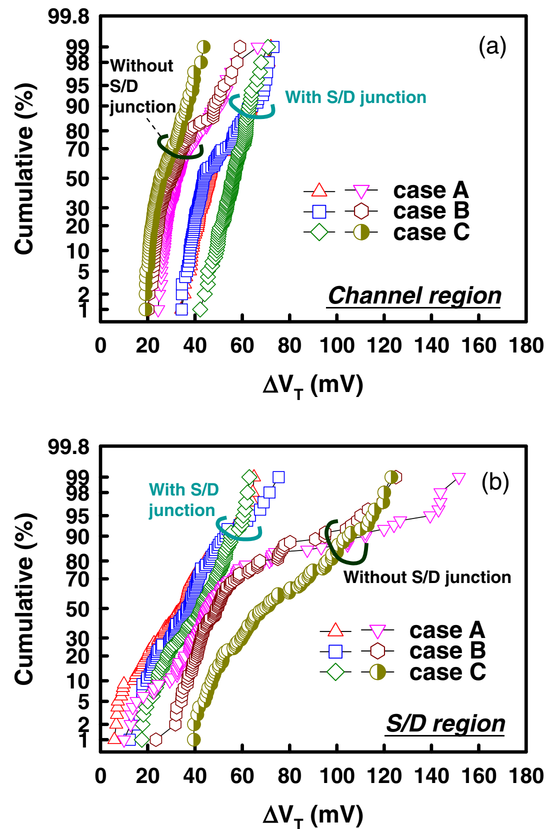

Fig. 11. (Color online) ΔV_T distribution of case A, case B, and case C in the (a) channel region and (b) S/D region.

junctionless cell, even though the cell geometry changes. To give insight into the origin of the tail bits shown in Fig. 11, Figs. 12(a) and 12(b) demonstrate the statistical contour plots of the ΔV_T as a function of single-trap position along the L- and W-directions, where a single-trap RTN is randomly placed in the channel and cell-to-cell S/D region. For the S/D junctionless cell, these figures clearly indicate that ΔV_T in the S/D region is significantly larger than that in the channel region. Moreover, for both cases A and B with and without an S/D junction, ΔV_T in the AA edge region is larger than that in the center of AA. This phenomenon can be explained by the electric field intensification and current crowding at the AA edges. For case C with and without an S/D junction, a high ΔV_T area moves from the AA edge towards the center area along the W-direction. Therefore, the magnitude of the RTN fluctuation amplitude heavily depends on the trap position along the L- and W-directions. Conventionally, the number of oxide traps in the S/D region is assumed to be larger than that immediately below the FG, which is attributed to the worse oxidation and post oxidation process conditions. However, the oxide trap density in the S/D region must be lowered to suppress RTN.

4. Conclusions

In this paper, we show that ΔV_T strongly depends on the lateral position of a trap over the active area. The obtained result allows us to highlight the importance of S/D region characteristics against RTN instabilities. We have presented, for the first time, the great influence of the S/D region on the RTN amplitude in NAND Flash. Considering the results of

© 2013 The Japan Society of Applied Physics

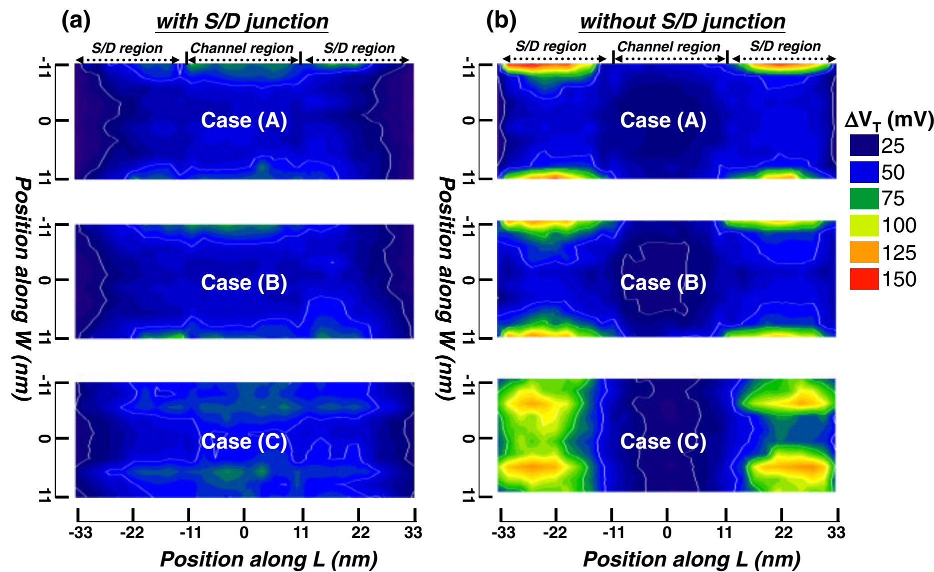

Fig. 12. (Color online) Statistical contour plots of ΔV_T distribution as a function of single-trap position along the L- and W-directions (a) with and (b) without S/D junction for cases A, B, and C.

RTN, the reduction in the number of surface states in the S/D region is crucial. The knowledge collected in this study will be useful to fix the V_T distribution widening by RTN for the further down scaled NAND Flash.

Acknowledgments

This work was supported in part by Taiwan National Science Council (NSC) under Contract 100-2218-E-009-026-MY3. The authors would like to thank Nina Mitiukhina and Tsai-Hao Kuo of National Chiao Tung University for their technical support.

1) P. Fantini, A. Ghetti, A. Marinoni, G. Ghidini, A. Visconti, and A. Marmiroli: IEEE Electron Device Lett. **28** (2007) 1114.
2) K. Prall and K. Parat: IEDM Tech. Dig., 2010, p. 101.
3) H. Kurata, K. Otsuga, A. Kotabe, S. Kajiyama, T. Osabe, Y. Sasago, S. Narumi, K. Tokami, S. Kamohara, and O. Tsuchiya: Symp. VLSI Technology Dig. Tech. Pap., 2006, p. 112.
4) K. Sonoda, K. Ishikawa, T. Eimori, and O. Tsuchiya: IEEE Trans. Electron Devices **54** (2007) 1918.
5) M. Tanizawa, S. Ohbayashi, T. Okagaki, K. Sonoda, K. Eikyu, Y. Hirano, K. Ishikawa, O. Tsuchiya, and Y. Inoue: Symp. VLSI Technology Dig. Tech. Pap., 2010, p. 95.
6) T. Nagumo, K. Takeuchi, T. Hase, and Y. Hayashi: IEDM Tech. Dig., 2010, p. 628.
7) K. Abe, A. Teramoto, S. Sugawa, and T. Ohmi: IEEE IRPS Tech. Dig., 2011, p. 381.
8) K. Fukuda, Y. Shimizu, K. Amemiya, M. Kamoshida, and C. Hu: IEDM Tech. Dig., 2007, p. 169.
9) C. Monzio Compagnoni, R. Gusmeroli, A. S. Spinelli, A. L. Lacaita, M. Bonanomi, and A. Visconti: IEEE Trans. Electron Devices **55** (2008) 388.
10) A. S. Spinelli, C. Monzio Compagnoni, R. Gusmeroli, M. Ghidotti, and A. Visconti: Jpn. J. Appl. Phys. **47** (2008) 2598.
11) H. Miki, T. Osabe, N. Tega, A. Kotabe, H. Kurata, K. Tokami, Y. Ikeda, S. Kamohara, and R. Yamada: IEEE IRPS Tech. Dig., 2007, p. 29.
12) A. Asenov, R. Balasubramaniam, A. R. Brown, and J. H. Davies: IEEE Trans. Electron Devices **50** (2003) 839.
13) A. Ghetti, M. Bonanomi, C. Monzio Compagnoni, A. S. Spinelli, A. L. Lacaita, and A. Visconti: IEEE IRPS Tech. Dig., 2008, p. 610.
14) A. Ghetti, C. Monzio Compagnoni, A. S. Spinelli, and A. Visconti: IEEE Trans. Electron Devices **56** (2009) 1746.
15) S. T. Martin, G. P. Li, E. Worley, and J. White: IEEE Electron Device Lett. **18** (1997) 444.
16) M.-H. Tsai, T. P. Ma, and T. B. Hook: IEEE Electron Device Lett. **15** (1994) 504.
17) R. Gusmeroli, C. Monzio Compagnoni, A. Riva, A. S. Spinelli, A. L. Lacaita, M. Bonanomi, and A. Visconti: IEDM Tech. Dig., 2006, p. 483.
18) Y. M. Kim, I. H. Cho, H.-I. Kwon, and J.-H. Lee: Jpn. J. Appl. Phys. **50** (2011) 114201.
19) C.-H. Lee, J. Choi, Y. Park, C. Kang, B.-I. Choi, H. Kim, H. Oh, and W.-S. Lee: Symp. VLSI Technology Dig. Tech. Pap., 2008, p. 118.
20) H.-T. Lue, E.-K. Lai, Y. H. Hsiao, S. P. Hong, M. T. Wu, F. H. Hsu, N. Z. Lien, S. Y. Wang, L. W. Yang, T. Yang, K. C. Chen, K. Y. Hsieh, R. Liu, and C.-Y. Lu: Symp. VLSI Technology Dig. Tech. Pap., 2008, p. 140.
21) T. Kim, N. Franklin, C. Srinivasan, P. Kalavade, and A. Goda: IEEE Electron Device Lett. **32** (2011) 1185.
22) C. H. Lee, I. C. Yang, C. Lee, C. H. Cheng, L. H. Chong, K. F. Chen, J. S. Huang, S. H. Ku, N. K. Zous, I. J. Huang, T. T. Han, M. S. Chen, W. P. Lu, K. C. Chen, T. Wang, and C.-Y. Lu: IEEE IRPS Tech. Dig., 2011, p. 534.
23) J.-H. Lee and S.-G. Jung: Microelectron. Reliab. **52** (2012) 662.
24) M. Ishiduki, Y. Fukuzumi, R. Katsumata, M. Kito, M. Kido, H. Tanaka, Y. Komori, Y. Nagata, T. Fujiwara, T. Maeda, Y. Mikajiri, S. Oota, M. Honda, Y. Iwata, R. Kirisawa, H. Aochi, and A. Nitayama: IEDM Tech. Dig., 2009, p. 625.
25) K.-T. Park, J.-S. Sel, J. Choi, Y. Song, C. Kim, and K. Kim: IEEE Trans. Electron Devices **55** (2008) 404.
26) W. Kim, Y. Kim, S. H. Park, J. Y. Seo, D. B. Kim, and B.-G. Park: Jpn. J. Appl. Phys. **51** (2012) 074301.
27) A. Ghetti, S. M. Amoroso, A. Mauri, and C. Monzio Compagnoni: IEEE Int. Memory Workshop, 2011, p. 91.
28) A. Ghetti, S. M. Amoroso, A. Mauri, and C. Monzio Compagnoni: IEEE Trans. Electron Devices **59** (2012) 309.
29) S. M. Amoroso, A. Ghetti, A. R. Brown, A. Mauri, C. Monzio Compagnoni, and A. Asenov: IEEE Trans. Electron Devices **59** (2012) 2774.
30) S.-M. Joe, J.-H. Yi, S.-K. Park, H. Shin, B.-G. Park, Y. J. Park, and J.-H. Lee: IEEE Trans. Electron Devices **58** (2011) 67.
31) S.-M. Joe, M.-K. Jeong, B.-S. Jo, K.-R. Han, S.-K. Park, and J.-H. Lee: IEEE Trans. Electron Devices **59** (2012) 3568.

 © 2013 The Japan Society of Applied Physics